Helix Self-Assembly from Anisotropic Molecules

Szilard N. Fejer and David J. Wales
University Chemical Laboratories, Lensfield Road, Cambridge CB2 1EW, United Kingdom
(Received 21 March 2007; published 24 August 2007)

We explore the potential energy landscape for clusters composed of disklike ellipsoidal particles interacting via an anisotropic potential based on the elliptic contact function. Over a wide range of parameter space we find global potential energy minima consisting of helices composed of one or more strands. Characterizing the potential energy surface in the region of helical global minima reveals a topology associated with "structure-seeking" systems. This result indicates that the helices will self-assemble over a wide range of temperature.

DOI: 10.1103/PhysRevLett.99.086106 PACS numbers: 81.16.Dn, 07.05.Tp, 34.20.Gj, 61.30.Cz

Designing fiberlike nanostructures with well-defined geometrical characteristics, including "supramolecular polymers," is an important contemporary research goal [1]. Computational modeling of self-assembling systems [2–7] can provide a better understanding of the various processes involved. In particular, insight into the structure, dynamics, and thermodynamics of such systems can be obtained by analyzing the underlying energy landscape [8–11]. Here we consider clusters composed of oblate (disklike) ellipsoids described by an anisotropic, Lennard-Jones-type potential [12]. We find that the global potential energy minima consist of helices for a wide range of relevant parameters. In fact, whenever the minimum energy for two interacting particles corresponds to a shifted stacked configuration, the global minima obtained for clusters exhibit long-range helical ordering. Furthermore, the corresponding potential energy landscapes exhibit a characteristic motif, which is known to support efficient self-assembly [4,9].

The Gay-Berne potential [13] is widely used for studying liquid crystals assembled from identical uniaxial ellipsoids [14]. Several related potentials have also been developed to provide a more flexible description of the interparticle interaction. In particular, the orientation- and distance-dependent elliptic contact function [15], $F(\mathbf{A}, \mathbf{B})$, supplies a mathematically exact way to determine the overlap of two arbitrary ellipsoids. Here

$$F(\mathbf{A}, \mathbf{B}) = \max_{\lambda} \min_{\mathbf{x}} \mathcal{S}(\mathbf{x}, \lambda) = \max_{\lambda} \mathcal{S}(\lambda), \tag{1}$$

where the $\mathbf{A}$ and $\mathbf{B}$ matrices are

$$\mathbf{A} = \sum_{i=1}^{3} a_i^{-2} \hat{\mathbf{u}}_i \otimes \hat{\mathbf{u}}_i, \qquad \mathbf{B} = \sum_{i=1}^{3} b_i^{-2} \hat{\mathbf{v}}_i \otimes \hat{\mathbf{v}}_i, \tag{2}$$

with $\hat{\mathbf{u}}_i$ and $\hat{\mathbf{v}}_i$ orthonormal unit vectors specifying the axes for ellipsoids A and B. "$\otimes$" denotes a dyadic product, and a_i and b_i are the lengths of the semiaxes of the two ellipsoids. The function $\mathcal{S}(\mathbf{x}, \lambda)$ is a combination of the ellipsoids written in quadratic forms:

$$\begin{aligned} \mathcal{A}(\mathbf{x}) &= (\mathbf{x} - \mathbf{r}_a)^T \mathbf{A} (\mathbf{x} - \mathbf{r}_a), \\ \mathcal{B}(\mathbf{x}) &= (\mathbf{x} - \mathbf{r}_b)^T \mathbf{B} (\mathbf{x} - \mathbf{r}_b), \\ \text{so that} \quad \mathcal{S}(\mathbf{x}, \lambda) &= \lambda \mathcal{A}(\mathbf{x}) + (1 - \lambda) \mathcal{B}(\mathbf{x}), \end{aligned} \tag{3}$$

where $\mathbf{r}_a$ and $\mathbf{r}_b$ are vectors defining the centers of ellipsoids A and B, with $0 \leq \lambda \leq 1$.

In the present work we employed the potential suggested by Paramonov and Yaliraki (PY)[12] with the form

$$V = 4\epsilon_0 \left[\left(\frac{\sigma_0}{r - rF_1(\mathbf{A}_1, \mathbf{B}_1)^{-1/2} + \sigma_0} \right)^{12} - \left(\frac{\sigma_0}{r - rF_2(\mathbf{A}_2, \mathbf{B}_2)^{-1/2} + \sigma_0} \right)^{6} \right], \tag{4}$$

where $F_1(\mathbf{A}_1, \mathbf{B}_1)$ and $F_2(\mathbf{A}_2, \mathbf{B}_2)$ are the "repulsive" and "attractive" elliptic contact functions, constructed using different shape matrices:

$$\mathbf{A}_1 = \sum_{i=1}^{3} a_{1i}^{-2} \hat{\mathbf{u}}_i \otimes \hat{\mathbf{u}}_i, \qquad \mathbf{B}_1 = \sum_{i=1}^{3} b_{1i}^{-2} \hat{\mathbf{v}}_i \otimes \hat{\mathbf{v}}_i$$

$$\text{and} \quad \mathbf{A}_2 = \sum_{i=1}^{3} a_{2i}^{-2} \hat{\mathbf{u}}_i \otimes \hat{\mathbf{u}}_i, \qquad \mathbf{B}_2 = \sum_{i=1}^{3} b_{2i}^{-2} \hat{\mathbf{v}}_i \otimes \hat{\mathbf{v}}_i,$$

where a_{1i} and b_{1i} are the lengths of the semiaxes of the repulsive ellipsoidal core for ellipsoids A and B, while a_{2i} and b_{2i} denote the lengths of the semiaxes for the attractive ellipsoidal core. The orientations of the attractive and repulsive ellipsoids are specified with unit vectors $\hat{\mathbf{u}}_i$ and $\hat{\mathbf{v}}_i$ for ellipsoids A and B and are the same for each particle. The above PY potential is different from the ellipsoid contact potential used by Perram *et al.* [16] because it becomes isotropic at large separations.

The most important parameters are ϵ_0, which determines the well depth for the pair interaction, and σ_0, which determines the width of the pair potential well (Fig. 1). σ_0 also governs the slope of the repulsive part of the potential: the repulsion is harder (steeper) for small values of σ_0 and softer for large values. Here σ_0 is employed as a variable so that the range of the potential can be studied for systems of particles with fixed sizes. Hence the dimensions

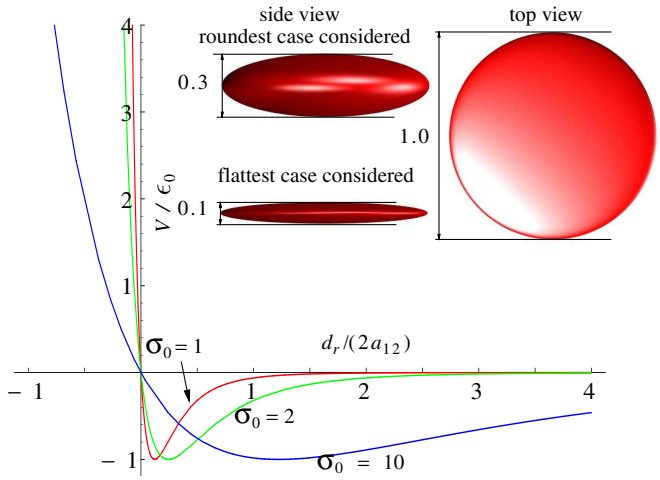

FIG. 1 (color online). The effect of σ_0 on the shape of the PY potential, for equal attractive and repulsive semiaxes. V is the potential energy and d_r is the directional distance for two ellipsoids, which vanishes whenever the two ellipsoids touch. The shapes of the repulsive ellipsoidal cores for the roundest and flattest particles considered are shown in the inset.

are defined in absolute units by parameters a_{1i} and a_{2i} with $i = 1, 2, 3$ for the semiaxis lengths of separate repulsive and attractive ellipsoids for each particle. With the well depth fixed at $\epsilon_0 = 1$ the parameter space for clusters of identical uniaxial ellipsoids consists of three variables: the main repulsive semiaxis length a_{11} ($a_{12} = a_{13} = 0.5$ are fixed), the main attractive semiaxis length a_{21} ($a_{22} = a_{23} = 0.5$ are fixed), and the well width parameter σ_0. Figure 1 shows how the shape of the potential changes with increasing σ_0 and the range of shapes investigated.

Global minima for clusters of ellipsoids were characterized using the basin-hopping approach, in which Monte Carlo steps are taken between minima of the potential energy surface [17,18]. To assess the reliability of the global optimization procedure we started at least five runs from random configurations at each size. If all the runs produced the same lowest minimum then this structure is our proposed global minimum. If the runs were not consistent, then the number of basin-hopping steps was increased and the searches repeated. In fact, with the parametrizations considered here only a few hundred basin-hopping steps were generally required for consistency between different runs, indicating that the potential energy surface has a simple form. We considered clusters containing between two and 55 ellipsoids and a wide range of parameters in the present work. The selected results illustrate our most important observations.

First we consider a parametrization that produces a lower energy for the side-by-side configuration relative to the face-to-face configuration. For systems containing more than ten particles the corresponding global minima consist of helices in which the principal axes of the discoids precess around the axis of the helix. A double helix is illustrated for 13 discoids in Fig. 2; some larger systems were found to exhibit triple helices.

Decreasing the repulsive part of the potential and shifting the minimum towards overlapping configurations favors face-to-face geometries relative to side-by-side structures. Particle overlap can be avoided by increasing the range parameter σ_0, which also smooths the underlying energy landscape reducing the number of low-lying minima, as for isotropic potentials [19]. For every parametrization in which the face-to-face orientation of the discoids is energetically favored over the side-by-side configuration, the cluster global minima were found to have helical symmetry. However, the main semiaxes of the particles are oriented parallel to the helical axis, in contrast to the structure in Fig. 2. Changing the parameters may change the geometry of the global minimum but does not change the helical topology.

The energies of enantiomeric left-handed and right-handed helices are identical for the PY potential because it has an achiral form. The emergence of helical order can be traced directly to destabilization of the perfectly stacked configuration for the dimer. This structure is actually a saddle point of Hessian index two for the parameter ranges in question. Hence we associate helix formation with symmetry breaking in the dimer, which leads to a shifted geometry for the latter system and ultimately to the emergence of helical order.

A wide exploration of the parameter space reveals that three main factors influence the structure of the helical

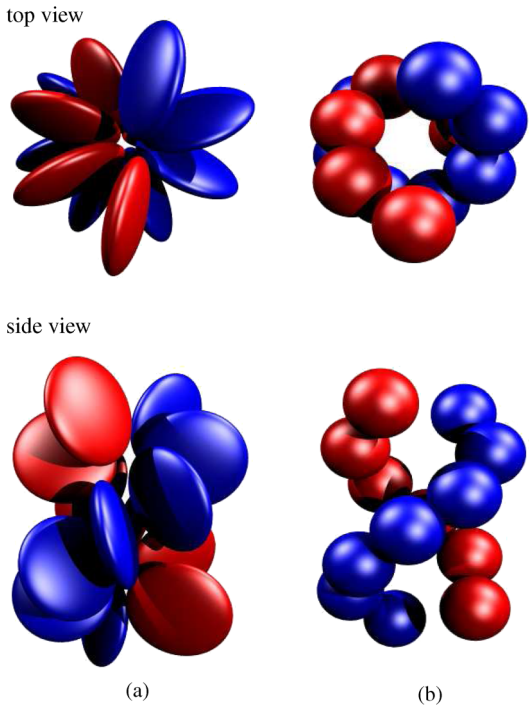

FIG. 2 (color online). Global minimum for a cluster containing 13 discoids interacting *via* the PY potential. (a) A double helical structure is preferred for a face-to-face/side-by-side strength ratio of 0.2 ($a_{11} = 0.15$, $a_{21} = 0.06$). (b) The same structure as in (a), but showing the double helical arrangement of the centers of the discoids.

global minima: namely, the interaction range (σ_0), the shape anisotropy, and cluster size. Decreasing σ_0 or increasing the particle shape anisotropy favors single-stranded geometries, while increasing the cluster size favors multiple strands. The radius of the helix can be increased by decreasing the repulsive main semiaxes of the particles, i.e., increasing the shape anisotropy of the particle. Figure 3(a) shows the global minimum of a 20-particle cluster composed of discoids with $a_{11} = 0.05$, $a_{21} = 0.4$, and $\sigma_0 = 18$. Figure 3(a) also shows the corresponding potential energy distribution of local minima encountered during basin-hopping global optimization.

To visualize the potential energy landscape we have constructed disconnectivity graphs [9,20]. This analysis involves calculating the transition states and pathways that connect local minima. At a regular series of values for the potential energy, V_α, the local minima are divided into disjoint sets, or "superbasins" [20]. Minima within each superbasin can interconvert without exceeding the threshold potential energy, but pathways between different superbasins must exceed the threshold. Each superbasin is represented by a point at the appropriate energy V_α on the vertical axis, and points for different V_α are joined if they share common minima. Lines terminate at the potential energy of each local minimum, which are arranged on the horizontal axis to produce the clearest representation. Systems corresponding to an efficient structure seeker exhibit disconnectivity graphs with a "palm tree" form [4,9,10] as in Fig. 3(c). This topology supports an unfrustrated free energy surface [8,9,11] with a single low-lying minimum that is kinetically accessible. This motif is therefore associated with efficient relaxation to the global minimum over a wide range of temperature [4,8–11]. The other low-lying minima also have varying degrees of helical character.

On increasing the number of ellipsoids complex helical structures start to emerge: double, triple, and quadruple helices become energetically more favored than single-stranded helices, depending on the size and the parametrization adopted. In each case the same putative global minimum was always found from a random initial configuration in a small number of basin-hopping steps (≤ 100). This result again indicates that the potential energy surface has a simple topology in each case. The global minimum of a 55-particle cluster with a quadruple helical geometry is depicted in Fig. 4. The helical character of the global minima is found to be a general feature of such clusters, independent of size, with the helical dimensions determined mainly by the length of the repulsive main semiaxis and the well width parameter σ_0. For example, the global minimum for the cluster in Fig. 3 becomes double stranded if the repulsive main semiaxis is increased. In general, multiple helices are favored by larger long-range attractive interactions.

Molecular self-assembling systems that are highly anisotropic in one dimension (supramolecular one-dimensional objects) often have helical symmetry [21].

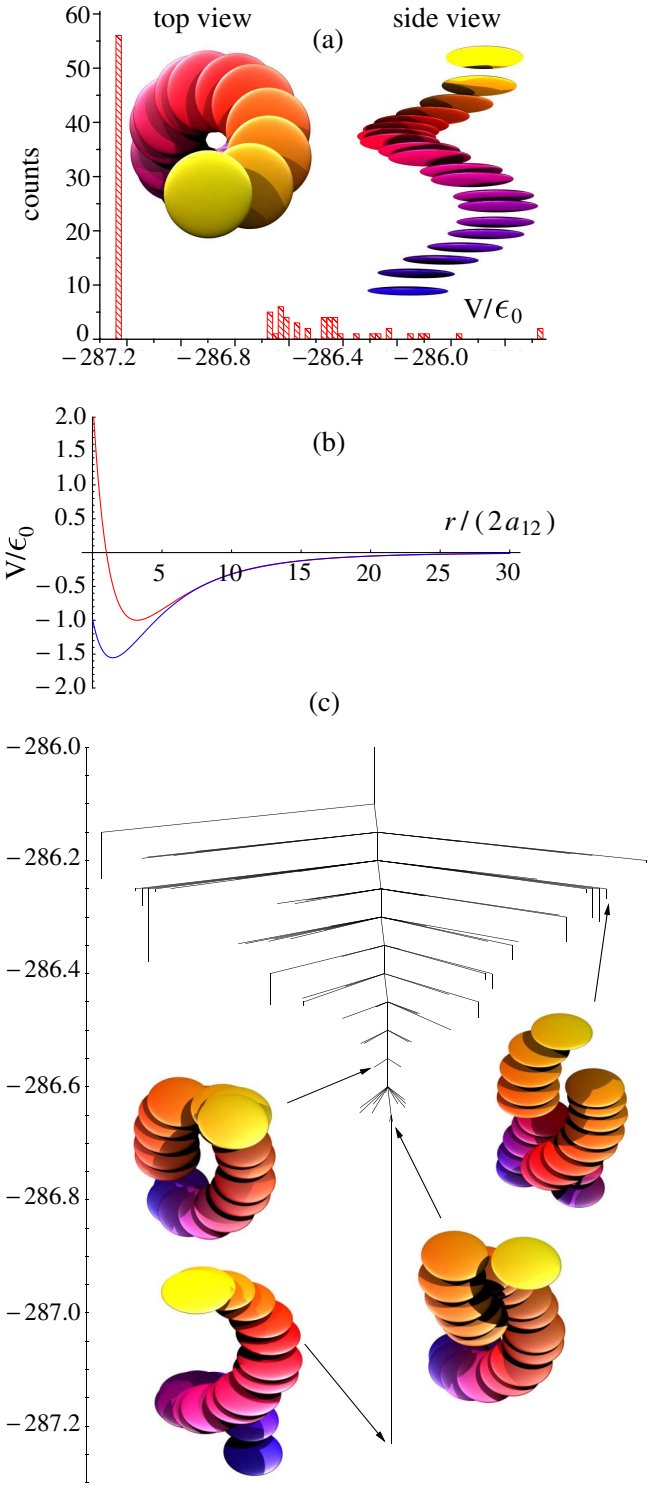

FIG. 3 (color online). (a) Probability distribution for the potential energy of local minima for a 20-particle cluster composed of particles with $a_{11} = 0.05$, $a_{21} = 0.4$, and $\sigma_0 = 18$. This distribution corresponds to the minima visited during 100 basin-hopping steps. Inset: helical structure of the global minimum for this system. (b) Face-to-face (blue curve) and side-by-side (red curve) interaction profiles as a function of the inter-center distance. (c) Disconnectivity graph for the same system, showing the organization of the landscape for the lowest 100 minima. Four of the minima are also illustrated.

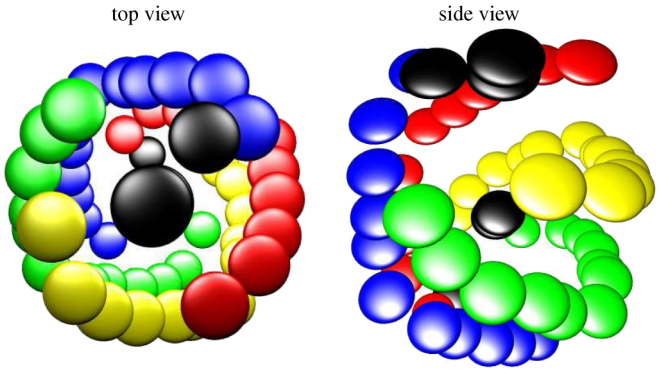

FIG. 4 (color online). Global minimum for a cluster assembled from 55 discoids with $a_{11} = 0.15$, $a_{21} = 0.4$, and $\sigma_0 = 30$. Each strand is colored differently. In this structure there are eight ellipsoids that cannot be assigned to any helical strand (colored in black): two in the middle of the cluster and three at both ends of the helices.

The building blocks of such helical objects can be bound by metal ligation, hydrogen bonding or aromatic π-π stacking [22,23]. Simple molecules such as oligopyridines [24] can act as helicating ligands for multivalent metal ions. Some coarse-grained models of chromatin fibres have also shown helical structures in which the neighboring nucleosomes stack onto each other in an offset mode [25,26]. A potential constructed to model wormlike polymer chains can reproduce helical ground states corresponding to polypeptide structures [27]. Some low-temperature helices have also been observed for clusters interacting *via* an isotropic potential, but these structures were stable only in a limited size range [28].

Recently it has been found that a certain discotic triester crystallizes in a single-stranded helical arrangement, in which the neighboring benzene rings are stacked in an offset fashion [29]. If this molecule were represented as a discoid, the preferred orientation of two molecules in the crystal would correspond to a shifted, stacked orientation, which is the preferred geometry for the potentials that we have considered here. Our results suggest that crystallization of the triester is a self-assembling process driven by long-range electrostatic interactions, which become anisotropic as the intermolecular distance decreases. The long-range interactions orient the discotic molecules in a parallel fashion, while shorter-range terms in the intermolecular potential fine-tune the structure, resulting in the observed shifted stacked configuration.

In summary, using the PY potential to model clusters of disk-shaped particles with long-range interactions, helical global minima were reliably located whenever the favored dimer geometry is a shifted stacked configuration. This simple diagnostic suggests a design principle that might be exploited in future work. Monodisperse systems containing disklike colloidal particles could perhaps be manipulated to self-assemble into helices by varying parameters such as the particle size and anisotropy. Our results indicate that for the efficient formation of helical structures, the primary requirements are particle anisotropy and long-range interactions that become anisotropic at small distances. Such systems not only possess helical global minima, but also exhibit potential energy landscapes that are known to result in reliable self-assembly over a wide range of conditions [4,9]. The corresponding systems are predicted to be both thermodynamically stable and kinetically accessible.

[1] J.-M. Lehn, *Supramolecular Chemistry* (VCH, Weinheim, 1995).
[2] A. W. Wilber *et al.*, arXiv:cond-mat/0606634.
[3] D. C. Rapaport, Phys. Rev. E **70**, 051905 (2004).
[4] D. J. Wales, Phil. Trans. R. Soc. A **363**, 357 (2005).
[5] M. F. Hagan and D. Chandler, Biophys. J. **91**, 42 (2006).
[6] K. Van Workum and J. F. Douglas, Phys. Rev. E **73**, 031502 (2006).
[7] T. Chen, Z. Zhang, and S. C. Glotzer, Proc. Natl. Acad. Sci. U.S.A. **104**, 717 (2007).
[8] J. N. Onuchic, Z. Luthey-Schulten, and P. G. Wolynes, Annu. Rev. Phys. Chem. **48**, 545 (1997).
[9] D. J. Wales, *Energy Landscapes* (Cambridge University Press, Cambridge, England, 2003).
[10] C. L. Brooks, J. N. Onuchic, and D. J. Wales, Science **293**, 612 (2001).
[11] C. M. Dobson, A. Šali, and M. Karplus, Angew. Chem., Int. Ed. **37**, 868 (1998).
[12] L. Paramonov and S. N. Yaliraki, J. Chem. Phys. **123**, 194111 (2005).
[13] J. G. Gay and B. J. Berne, J. Chem. Phys. **74**, 3316 (1981).
[14] S. Chandrasekhar and G. S. Ranganath, Rep. Prog. Phys. **53**, 57 (1990).
[15] J. W. Perram and M. S. Wertheim, J. Comput. Phys. **58**, 409 (1985).
[16] J. W. Perram, J. Rasmussen, E. Præstgaard, and J. L. Lebowitz, Phys. Rev. E **54**, 6565 (1996).
[17] Z. Li and H. A. Scheraga, Proc. Natl. Acad. Sci. U.S.A. **84**, 6611 (1987).
[18] D. J. Wales and J. P. K. Doye, J. Phys. Chem. A **101**, 5111 (1997).
[19] J. P. K. Doye and D. J. Wales, J. Phys. B **29**, 4859 (1996).
[20] O. M. Becker and M. Karplus, J. Chem. Phys. **106**, 1495 (1997).
[21] J. D. Hartgerink, E. R. Zubarev, and S. I. Stupp, Curr. Opin. Solid State Mater. Sci. **5**, 355 (2001).
[22] L. Brunsveld *et al.*, Proc. Natl. Acad. Sci. U.S.A. **99**, 4977 (2002).
[23] H. Engelkamp, S. Middelbeek, and R. J. M. Nolte, Science **284**, 785 (1999).
[24] E. C. Constable, Tetrahedron **48**, 10 013 (1992).
[25] G. Wedemann and J. Langowski, Biophys. J. **82**, 2847 (2002).
[26] J. Langowski, Eur. Phys. J. E **19**, 241 (2006).
[27] J. P. Kemp and Z. Y. Chen, Phys. Rev. Lett. **81**, 3880 (1998).
[28] J. E. Magee, V. R. Vasquez, and L. Lue, Phys. Rev. Lett. **96**, 207802 (2006).
[29] I. Azumaya *et al.*, Angew. Chem., Int. Ed. Engl. **43**, 1360 (2004).